RevMexAA (Serie de Conferencias), **2**, 27-35 (1995)

THE INNER CORE OF η CARINAE IN THE NEAR INFRARED

F. Rigaut
Canada-France-Hawaii Telescope, P.O. Box 1597, Kamuela, HI 96743, USA

and

G. Gehring
European Southern Observatory,
Karl-Schwarzschild-Strasse 2, D-85748 Garching bei München, Germany

RESUMEN

Se presentan resultados de observaciones *JHKL'M* de la parte central de η Car realizadas con los instrumentos de óptica adaptativa COME-ON y COME-ON+, con resoluciones entre 0.1″ y 0.25″. Estas observaciones muestran la estructura de la parte central de la nebulosa, que incluye un torus equatorial y *shells* de polvo alrededor de la estrella. No se detectaron componentes estelar, pero se detectó un exceso infrarrojo muy cerca de la estrella central ($\geq$ 100 UA) que interpretamos como la emisión de polvo a temperatura $\simeq$ 1000 K.

ABSTRACT

JHKLM observations of the central part of η Carinae (5″ × 5″), obtained with the adaptive optics systems COME-ON and COME-ON+, are reported at angular resolutions between 0.1″ and 0.25″. These observations show the very complex structure of the core, which includes an equatorial torus, shells of dust around the central object, and a jet like structure. No evidence of multiplicity is found. We show that a component with a temperature $\simeq$ 1000 K (most probably dust) is present within 100 AU of the central star.

Key words: **CIRCUMSTELLAR MATTER — STARS: INDIVIDUAL: (η CAR)**

1. INTRODUCTION

η Car has been the subject of intensive —and sometime passionate— studies since the last century, because of its very peculiar characteristics: These include, among others, a huge luminosity ($\sim 5 \times 10^6\ L_\odot$), the outburst in the 1840's, a high infrared excess, a large mass (probably more than 100 $M_\odot$), an unusual mass loss ($\sim 10^{-2}\ M_\odot\ \mathrm{yr}^{-1}$), a bipolar structure and a material large ejection velocity ($\sim$ 500 to 1000 km s^{-1}). η Car is an excellent candidate for diffraction–limited imaging at infrared wavelengths due to its size and its high astrophysical interest (Bensammar et al. 1985; Perrier, Chelli, & Zinnecker 1987).

We have adopted a distance of 2500 pc for η Car. In the following we considered the model of the bi-lobes for the geometry of the homonculus, with a main axis at PA $\simeq$ 132° and an equatorial plane perpendicular to that.

In § 2, we describe the observation techniques and the data processing. In § 3 we presents our *JHKL'M* observations of the central 5″ of the homonculus while in § 4, we get closer to the source and investigate the inner 1.7″ in some details and report on photometry of some outstanding features. In § 5 we briefly summarize and discuss the results.

2. OBSERVATIONS AND REDUCTION PROCEDURES

2.1. Adaptive Optics and the COME-ON System

Atmospheric turbulence severely limits the spatial resolution achievable from ground based telescopes. By sensing and correcting in real time the wavefront distortion, adaptive optics (AO) restores the full imaging capabilities of large telescopes and allows diffraction–limited imaging (Merkle 1986). The COME-ON adaptive optics prototype for the Very Large Telescope (Kern et al. 1990), developed by ESO, Observatoire de Paris–Meudon, ONERA and Laserdot, has been tested successfully in 1990 and 1991 and has demonstrated the dramatic improvement in image quality achieved by this technique (Rousset et al. 1990; Rigaut et al. 1991): images as sharp as 0.10″ were routinely obtained at near infrared wavelengths (Rigaut et al. 1992).

The COME-ON system was installed at the Cassegrain focus of the ESO 3.6-m telescope. The deformable mirror was a continuous facesheet mirror with 19 piezoelectric actuators. A separate two-axis mirror compensated for the overall wavefront tilt. Both mirrors were driven by a digital control loop. The Shack Hartmann wavefront sensor sampled the wavefront deformations using 20 subapertures on a 5 × 5 grid. The sampling rate was 100 Hz and the frequency response of the closed–loop was 25 Hz.

The IR imaging camera was a 32 × 32 InSb array (Lacombe et al. 1989) with a 0.1 or 0.05 arcsec pixel size on the sky. The camera was read-out noise limited, with $\sigma_e \simeq 3000\ e^-$. Images were recorded at the standard IR photometric wavelengths: J (1.2 μm), H (1.68 μm), K (2.23 μm), L' (3.87 μm) and M (4.75 μm).

2.2. Observations and Data Processing

η Car was mapped in the near infrared filters J, H, K, L' and M in January and April 1991. The star itself was used as a reference for wavefront sensing. The images were diffraction–limited at K, L' and M (FWHM of 0.13″, 0.21″ and 0.25″ respectively).

Images were processed using the standard method of bias subtraction and flat field correction. To get the large field shown in § 3, 5 processed frames were combined in a mosaic (except for the K image, see below).

In all cases, a main sequence star was imaged before *and* after η Car was observed, in order to calibrate the point spread function (PSF) of the system. This PSF was later used for a-posteriori processing to deconvolve the images of η Car in order to get rid of the residual aberrations not completely corrected by the system and the large halo characteristic of the adaptively corrected images (Rigaut et al. 1992). The Lucy-Richardson deconvolution method was used for all images shown in this paper, but we also compared the results with other methods such as CLEAN, Maximum Entropy and Maximum Likelihood. All methods give similar results. η Car was observed on several occasions (and subsequently with the COME-ON+ system, upgraded version of COME-ON) with identical results, which made us very confident in the quality of the data and of the image processing.

3. THE CENTRAL HOMONCULUS

The central part of the homonculus has been investigated throughout the spectrum, most notably in the visible (*Hubble Space Telescope* images), the near-infrared (Allen 1989), and the mid-infrared (Hackwell et al. 1986; Hyland et al. 1979). Whereas the dramatic *Hubble Space Telescope* images provide some valuable information about the geometry of the whole nebula, the near infrared images probe more deeply into it, showing that it is hollow, and optically thin in this domain ($\lambda \geq 2.2\,\mu$m), strengthening the model of thin and empty lobes. Allen's images show an elongation of the central emission along an axis parallel to the minor axis of the nebula, i.e., in what could be called the equatorial plane in the "double lobes" model (see Duschl et al. 1995). This elongation was in fact resolved at longer wavelength by Hackwell (1986) and Hyland (1979) into two components, separated by 1.9″, of similar intensity at $\simeq 12\,\mu$m. These showed that the second component, away from the central object, was of much lower apparent temperature.

Figure 1 shows the central 5″× 5″ of the Homonculus at K, L' and M. The L' and M images were obtained with COME-ON as described in the previous section. The K image has been recorded more recently (April 1994), using the COME-ON+ system (Rousset et al. 1993) at ESO and a 256 × 256 Nicmos Camera developed and operated by the Max-Planck Institute at Garching, Germany.

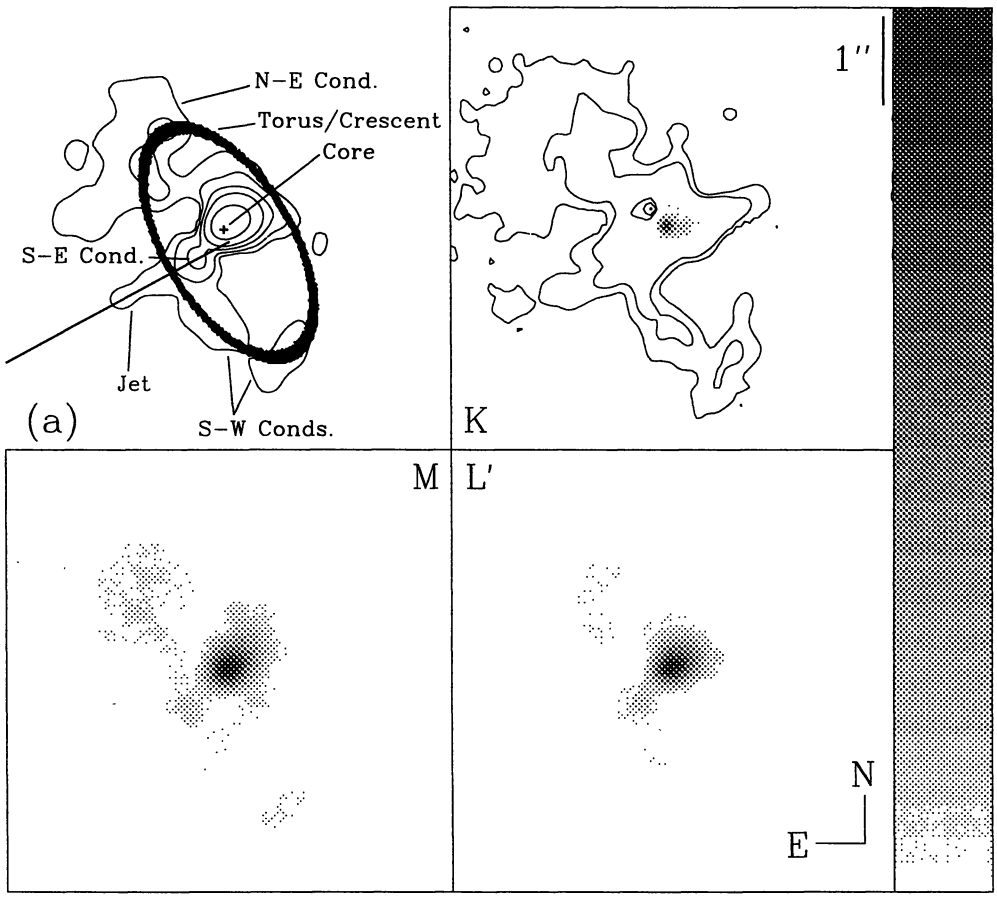

Fig. 1. Central 5″× 5″ of the Homonculus at *K*, *L'* and *M*. The intensity greyscale at the right range from 1.2 10^{-2} of the maximum to the maximum intensity. Each image maximum is normalized to the same intensity for display purposes. The contour lines in the *K* images are at 5 × 10^{-4} and 15 × 10^{-4} of the image's maximum. They are plotted to show the similarity of the very low surface brightness *K* features with the *L'* and *M* emission. The upper left figure defines the notation used throughout the text. It also indicates the torus/crescent structure discussed in § 3 and the axis of the jet.

Figure 1 suggests several remarks:

1. The emission shows intricate and complex structures, as already noted by Allen (1989). It *is* clumpy.

2. The similarity with the already published images mentioned above is obvious. Here, however, the resolution is 4 to 8 times better and we can note that the emission is mostly located along the Homonculus minor axis. Also, the nature of the double source quoted by Hyland et al. and Hackwell et al. is clearly revealed: The secondary component is here separated into several sources, forming a cluster of (dust) condensations at the location observed by the above authors (distance to the central source $\simeq$ 1.5″, PA $\simeq$ 53°).

3. Although fainter on the SW side, there seems to be a symmetry about the major axis of the Homonculus, at PA $\simeq$ 135°. It should be noted here that Hackwell et al. found a peak in the optical depth in the SW side of the central source. The value they quote for the optical depth at 9.7 μm corresponds to $\tau \simeq 0.5$ at 4 μm, which may partially explain the intensity asymmetry.

4. The 3 wavelengths exhibit very similar features, although the ratio of the different components may vary. One can identify at least two "temperature" components: The central object, and the surrounding nebula. A third component is the emission in the immediate vicinity of the central source (distance $\leq 0.3''$), as detailed in § 4.

5. The central source is largely resolved in *L'* and *M*, and is elongated along a PA $\simeq 135°$.

6. Other prominent features are the SE condensation, $\simeq 0.55''$ from the central object and at a PA $= 137° \pm 2°$, and a jet like feature, visible in all 3 images, extending at least $1.5''$ SE from the central star, at a PA $\simeq 126°$. It has to be noted that this jet does not point towards the central object (it misses it by $0.25''$).

It is still difficult from these images to decide on the actual morphology of the source at the scale of $1''$–$3''$. There are at least two interpretations for the **equatorial emission**:
(a) This could be an indication of a torus of dust, with an inner radius of $1.1''$ or 2800 AU and an outer radius of $1.5''$ or 3800 AU. Assuming this torus is circular, the ratio of the minor and major axis leads to an inclination of $27° \pm 5°$ of the plane of the torus with respect to the line of sight. This interpretation is in accordance with the model proposed by Warren-Smith et al. (1979), who deduced the same physical parameters from polarization observations at visible wavelengths.
(b) This crescent (arc) shape, or double crescent shape, could be an effect of optical thickness within the "walls" of the lobe cavity. Indeed, if the lobes are hollow, the projected mass may have quite sharp edges, and result in a larger emission in the infrared where it is optical thin.
However, the fact that the SE part of the torus/arc is much brighter than the NW part (which is, in fact, almost non-existent) is not easily understandable in either model. In fact it should be fainter because the main axis of the nebula, in the bi-lobes model, is supposed to be inclined to the plane of the sky by 20–30°, with *the North-Western part tilted away from the observer*. Therefore, the NW part of the torus/arc should be closer to the observer and should suffer a lower extinction.

The main-axis jet structure is also intriguing: it adds another puzzle to this object, for which two kinds of mass ejection are already coexistent on larger scales (the large blobs and the North-Eastern jet+bow shock).

From the 3 color maps, we have been able to determine a color temperature. Following the example of Allen (1989), we assumed an emissivity $\epsilon_\lambda \propto \lambda^{-1}$, and found temperature values from 350–400 K ($0.5''$ from the star) to 300 K at $2''$ (NE and SW condensations).

The temperature and morphology even closer to the central source ($<0.5''$) may be crucial elements for the understanding of the physical and dynamical properties of the object. In view of the *L'* and *M* images, we can already say that the central source is resolved at these wavelengths, so we are most probably seeing hot dust around and close to the central object. These points are examined in more detail in the next section.

4. THE INNER CORE

Due to its complexity, η Car has not been an easy object to observe with what were until recently classical high resolution techniques. Speckle imaging is more efficient on objects featuring several point sources (up to a dozen) but is not very well suited for work on extended objects (although recent developments have greatly improved that situation). However, successful work has been done by Weigelt & Ebersberger (1986) in the visible, and showed a resolution of the central source into 4 components, all within a diameter of $0.2''$.

In the infrared, Bensammar et al. (1985) used an original techniques combining imaging of the source through a spatial filter and image reconstruction using inverse Hadamar transforms. They found that the core is extended in the near infrared, with a full–width at 1/e intensity of $0.13''$ from *J* to *L* and of 0.23 at *M*. They interpreted these results as evidence for the inner layer of the dust envelope. We will see in this section that our results support this interpretation with only slight variations.

Figure 2 shows the very inner core ($1.6'' \times 1.6''$) of the nebula. These images were taken in April 1991. The PSF was very stable at *K*, *L'* and *M* and the deconvolution/desapodisation process proceeded very well for these wavelengths. In *J*, the PSF is intrinsically less stable in time, and the correction performed by the AO system is not as good as at longer wavelengths. We suspect that the *J* image may therefore suffer from residual artifacts (for instance, the diamond shaped central object may not be real), although the global shape and characteristics are certainly true (the comma shape to the North is seen in the visible by the *HST*).
Examination of Figure 2 highlights the following points:

1. In J, the core is basically a point source surrounded by a diffuse emission region, slightly elongated along the major axis of the homonculus. The diffuse emission is the signature of scattered light by gas or dust. A comma shape structure is visible NE from the central source. This feature is conspicuous in the *Hubble Space Telescope* images (Weigelt, private communication) and is also attributable to scattering.

2. At J and K, most of the flux (45% and 55% respectively within 0.26″, see next section) comes from the unresolved very central object.

3. At K, the elongation along the Homonculus major axis is even more pronounced. At this wavelength, except for the central star, all emission is from dust grains. The emitting region has a bipolar shape, fairly axi-symmetric (about PA $\simeq$ 135°), if not centro-symmetric, except the SE pole is fainter than the opposite one. Another important feature is the shell located (0.22″$\pm$ 0.02″) NW from the central source. The shell is basically unresolved in width. This bipolar structure plus "thin" shell is reminiscent the structure at larger scale, i.e., the large, regular and thin lobes of the Homonculus. This alone suggests either that mass loss is an ongoing process or that material was ejected in the past with a large velocity dispersion, leading to high velocity material flowing away at several hundred of kilometers per second while other material moves at only 20–30 km s^{-1}. This last interpretation is supported by the fact that (a) Weigelt component BCD proper motion corresponds to tangential velocity of 30 km s^{-1} (also their proper motions are radial, i.e., the velocity vectors point away from the central star, which rules out the

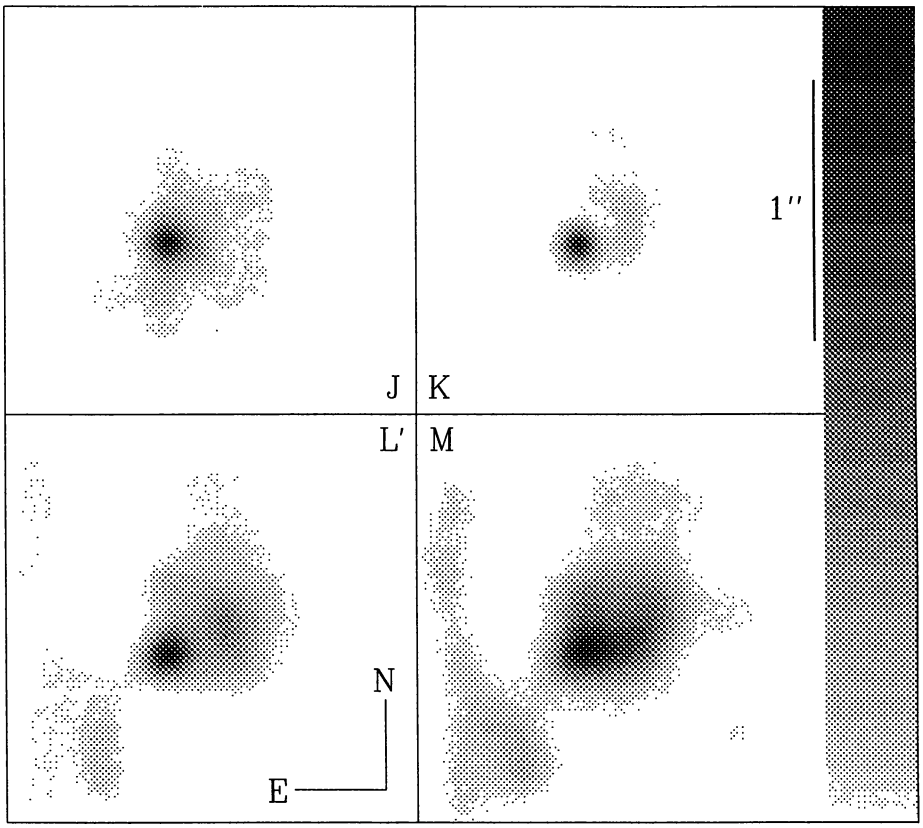

Fig. 2. Inner core of η Car at J, K, L' and M. Each image is 1.6″× 1.6″ (4000 AU × 4000 AU). Scattering is predominant at J. The K image, and especially the L' and M images show the emission of dust at high (700 K) to medium (350 K) temperature, decreasing gradually outwards from the central object. Shells of material are clearly seen in K and L', NW from the star, together with a condensation SE of it.

multiple star hypothesis [Weigelt et al. 1995]) and (b) we do not see any measurable difference ($\leq 0.05''$) in a 2 years period, at least at the SE condensation and the NW shell positions. We would like to note here that the NW shell does not seem to be directly related to Weigelt BCD object.

4. At *L'* and *M*, the dust at distance $> 0.15''$ dominates the emission. The central object begins to fade, while the shell emission is increasing. The SE condensation also appears (it is already visible at *K*, but very faint because of its low temperature $\simeq 400$ K, cf., previous section). Except the extension on the NE corner, the emission is still fairly symmetric.

5. Because of the better spatial sampling, one can see on these images that the SE condensation is not a point source.

6. There is no evidence of a stellar companion at *K* ,*L'* and *M*. This also appears to be the case at *J*, but at this wavelength the quality of the reconstructed image prevents unambiguous detection, so that no conclusion can be reached. In any case, Weigelt has demonstrated that his B, C and D components were not stars, but gas clumps (Weigelt et al. 1995). If we assume simple scattering, the contrast between A and B, C and D should increase at longer wavelengths, making the detection difficult at *J* and *H* bands.

7. At *K*, *L'* and *M*, the emission is "squeezed" at about $0.15''$ SE from the central source. This may well be a direct indication of the collimating mechanism. If so, this mechanism must be quite efficient, at least on small scales, to prevent the material from flowing away at the sides.

4.1. Photometry

From these images of the very central core, we have been able to derive photometric figures. Due to a lack of a suitable calibration, it has not been possible to obtain absolute photometry, but we have been able to derive color indices. We find J–$K = 2.75$, H–$K = 1.62$, K–$L' = 2.29$ and K–$M = 3.53$ for a $1.4''$ square mask computed to match the mask used by Allen (1989) for his photometry of the central source. Those values are within 0.1 magnitude of the values given by Allen. The absolute photometry was then derived to match the m_K given in this paper (the *K* image was filtered by the above mentioned mask).

We were then able to complete aperture photometry on selected parts of the field. The results are presented in Figure 3. The lower right image shows the *L'* image (same as Fig. 2), where we have superimposed the position of the masks in which the flux was integrated. Mask#1 is $0.26''$ in diameter, centered on the central object. Mask#2 covers the first shell, while mask#3 covers the outer NW area. C1 is centered on the SE condensation, $0.5''$ from the central source. The covered surface areas are 0.055, 0.152, 0.376 and 0.289 square arcseconds respectively. The illustrated spectra are *not* normalized by the emission solid angle.

The errors in the spectra come mainly from errors induced by the deconvolution processes. This was carefully estimated by measuring the standard deviation using different deconvolution methods applied on a number of object frames and PSF frames. A factor has been applied to the results to account for undetermined sources of error and we believe it is quite conservative. The values were finally corrected for extinction (taking $A_J = 0.80$ and $A_\lambda \propto \lambda^{-2}$, Davidson 1971).

4.1.1. Central Source #1

At this stage, we obtained a spectrum for mask#1 that shows a large infrared excess of J–$K = 2.4$. This is obviously not compatible with stellar emission alone. Assuming all the flux in *J* is emitted by a star in the range of temperature expected for η Car ($T \geq 7000$ K), which is in the Rayleigh–Jeans domain of emission, the star would account for only 10% of the flux observed in *K*. What can be the reasons of this discrepancy?

- The adopted extinction law is not valid, and we have instead an extremely abnormal extinction law. This does not seem reasonable, and no extinction law that we are aware of could explain such a J–K given the measured A_V.
- There may be very strong emission lines. This is ruled out by spectra taken by Whitelock et al. (1983) and Allen et al. (1985). Even integrated on a $12''$ diameter aperture, these lines —although strong— are negligible compared to the continuum; it affects $\log(f_\lambda)$ by -0.0409,

-0.0177, -0.0066 in J, H, and K respectively. This is too small a contribution to significantly change the J–K color index, even assuming an unusual distribution of the line emission regions. However, the emission line contribution has been subtracted from the spectra of Figure 3.

- There may be absorption lines close to the central source that reduce significantly the flux at J. This seems unlikely, given the optical thickness that would be required. Beside, the emission lines detected by Allen et al. and Whitelock et al. are recombination lines (H and He mainly), so the presence of strong absorption lines does not seem probable.
- This K excess could be radiated by another source. As the other hypothesis face severe problems, this seems the most likely one and we shall investigate it in more detail in the following.

Continuing the analysis of the spectrum of the central object on the basis of this hypothesis, we can measure the temperature of the additional component. A model with two components including a stellar contribution in $\log(f_\lambda) = -4\log(\lambda)$ (Rayleigh–Jeans) and a grey body of emissivity $\epsilon_\lambda = \lambda^{-1}$ at temperature $T = (1000 \pm 100)$ K can be fitted to the data with very good results. The subtraction reveals a third component at $T \simeq 300$ K, omnipresent throughout the whole nebula as found by Allen (1989). The smooth solid curve superimposed to #1 spectrum in Fig. 3 is the sum of these three contributions.

This leads us to the conclusion that *there is, within 0.1″ of the central star, "something" that radiates as a grey body at* $T \simeq 1000$ K.

Assuming a distance of 2500 pc for η Car we find a lower limit for the emissivity of 0.2. The actual emissivity is probably larger than this value, given that the central emission peak is not resolved at K, which means that whatever this additional component is, it is much more compact than the diffraction limit, and therefore also the mask aperture. In turn, the assumption of an emissivity $\epsilon_\lambda = \lambda^{-1}$ is probably not correct. However, trials to fit a black body instead of a grey body have been performed with success and give as good a fit with $T = (1250 \pm 100)$ K. Calculation of the luminosity of this object yields to $L \simeq 4 \times 10^4\ L_\odot$.

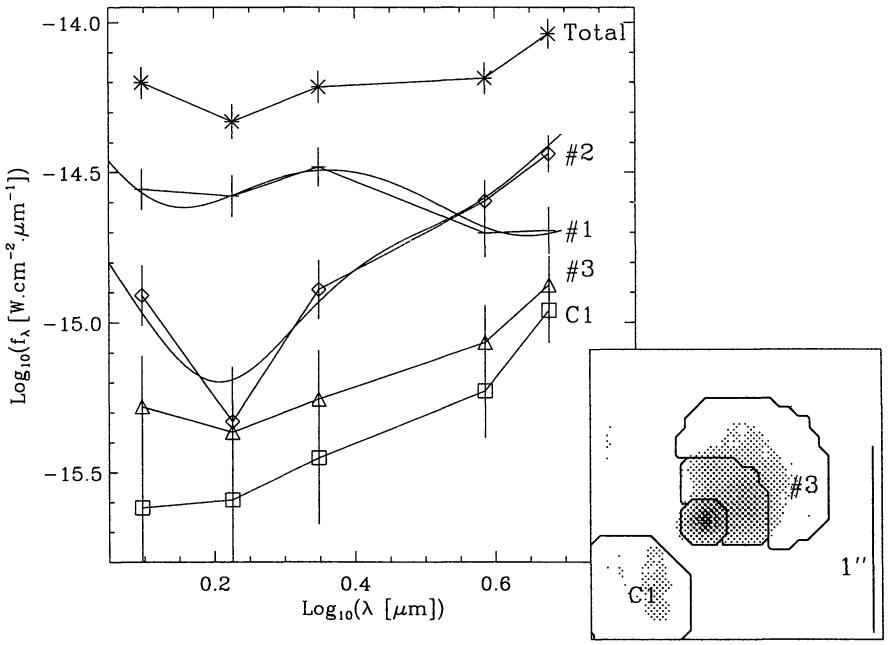

Fig. 3. Spectro-photometry of the different components of the core: The spectra of several regions, integrated over the masks shown on the lower right corner image, are plotted. The image is the L' image of Fig. 2. The masks have been chosen to cover the central star, the first NW shell, the outer shell(s) and the SE condensation. These spectra are corrected for extinction and the contribution from emission lines has been subtracted, as reported in the text. An attempt has been made to fit the emission of the mask#1 and #2 with three components and shows the presence of material that emits like a grey body at temperature T $\simeq$ 1000 K close to the central star.

What can be the nature of this additional object radiating at such a temperature? It is clearly too cold to be stellar. The other possibilities may be (a) an accretion disk that may have formed from the recent massive mass outflows (see contribution by Duschl et al. 1995), or (b) the inner layer of a dust envelope. This last hypothesis will fit quite well with the temperature expected for dust grain formation (1000–1500 K). Given some assumptions on the grain properties (radius of 0.5 μm [Men'shchikov 1989], $\rho = 1.5$ g cm^{-3}, $Q_a(2.2\ \mu\text{m}) = 0.1$), we compute a total mass of the emitting dust of $M_d = 10^{-6}\ M_\odot$. Taking material ejection velocities of 500 km s^{-1}, a dust-to-gas ratio of 0.01 and an emitting region of 0.04″ in diameter (100 AU), we derive a mass loss rate of $\dot{M} \simeq 10^{-3}\ M_\odot$ yr^{-1}, a value which is in good agreement well with independent estimates (van Genderen & Thé 1984; Hyland et al. 1979; Andriesse et al. 1978; Davidson 1989).

The assumed ejection velocity is backed up by P Cyg profiles commonly observed in the nebula. However, it is in contradiction with the tangential velocities derived by Weigelt from the proper motion of his components BCD.

4.1.2. Shell #2 and Outer Condensations

Following the same procedure, the spectra of the inner shell #2 can also be fitted with 3 components: scattered stellar light, a grey body and another grey body at a fixed temperature of 300 K. We find a temperature of 720 K for the shell dust component (0.2 arcsec from the star), a luminosity of $5 \times 10^4\ L_\odot$, and a mass of $5 \times 10^{-6}\ M_\odot$ (same assumptions as above). Again, the fitted spectra is superimposed to the spectra of #2.

Temperatures were derived for #3 and C1 using the $L'-M$ color index, leading to a value of (330 ± 30) K.

5. DISCUSSION AND CONCLUSION

Gathering all the information about η Car to produce a physical and morphological model has never been a trivial problem. The new data reported in this paper do not make it any easier. We have shown that:

- At a scale of 2500–10000 AU from the central star the dust is accumulated in the equatorial area at PA $\simeq 30°$.
- The NE condensation noticed by previous observers is a group of dust condensations with a T $\simeq$ 300 K.
- At a scale 100–2500 AU from the central source, the symmetry is similar to that of the homonculus: a bipolar structure, made out of thin shells/lobes of dust directly detected down to 500 AU of the star ($T_{dust} \simeq 700$ K at 500 AU).
- There is a conspicuous infrared excess within a region of 500 AU centered on the star (J–K = 2.4) that can not be explained by extinction or line emission/absorption alone. The *JHKL'M* photometry can be well approximated by a stellar component plus a grey body with T $\simeq$ 1000 K.

It is interesting to note that the detection of dust so close to the star is in contradiction with the existing models of dust formation around η Car. Andriesse (1978) quoted a grain formation radius of 2500 AU (although he noted that the gas density was too low at such a distance to allow grain formation). Men'shchikov (1989) gets a smaller value (650 AU or 0.26″) and his model is consistent with a dust temperature of 800 K at 0.3″. In the later model, the shell we detected at 0.2″ would be the inner edge of the envelope, and therefore the grain forming region. However, dust can not be formed at a distance smaller than 0.25″ from the star in his model, and therefore it can not explain the central IR excess.

Whether or not the mass outflow is continuing is another question. As we already mentioned, there is great uncertainty in the material velocity at the center in the nebula. P Cyg profiles and proper motion of the outer ejecta lead to velocities of 500 to > 1000 km s^{-1}, whereas proper motions measured from Weigelt components BCD give approximately 30 km s^{-1}. Therefore, the NW dust shell at 500 AU may or may not be a recent ejecta.

A key to solve this problem is the regular monitoring of the source at high resolution. Already, comparisons with 1D speckle data taken in 1981 (Perrier 1986) appear to indicate some changes, although we have not been able to derive quantitative values. Images taken with adaptive optics over a 10 year period should permit to detect proper motion in the dust envelope surrounding η Car. Integral field spectroscopy (in the visible, and when available, in the infrared) is also a must for this object, to get the 2D velocity distribution.

We would like to acknowledge the effort and success of the COME-ON and COME-ON+ teams. FR wants to thank Prof. P. Léna for his help during the physical interpretation process, together with Dr. W. Duschl and Prof. G. Weigelt for fruitful discussions during the La Plata workshop. We are also grateful to D. Bohlender for reading this paper and correcting our English.

REFERENCES

Allen, D.A. 1989, MNRAS, 241, 195
Allen, D.A., Jones, T.J., & Hyland, A.R. 1985, ApJ, 291, 280
Andriesse, C.D., Donn, B.D., & Viotti, R. 1978, MNRAS, 185, 771
Bensammar, S., Letourneur, N., Perrier, F., Friedjung, M., & Viotti, R., 1985, A&A, 146, L1
Davidson, K. 1971, MNRAS, 154, 415
_____. 1989, in Physics of Luminous Blue Variables, IAU Coll. No. 113, ed. K. Davidson, A. Moffat, & H. Lamers (Dordrecht: Kluwer), p. 101
Davidson, K., Dufour, R.J., Walborn, N.R., & Gull, T.R. 1986, ApJ, 305, 867
Duschl, W.J., Hofmann, K.-H., Rigaut, F., & Weigelt, G. 1995, RevMexAASC, 2, 17
Hackwell, J.A., Gehrz, R.D., & Grasdalen, G.L. 1986, ApJ, 311, 380
Hyland, A.R., Robinson, G., Mitchell, R.M., Thomas, J.A., & Becklin, E.E. 1979, ApJ, 233, 145
Kern, P., Rigaut, F., Léna, P., Merkle, F., & Rousset, G. 1990, SPIE, 1237, 345
Lacombe, F., Tiphène, D., Rouan, D., Léna, P., & Combes, M. 1989, A&A, 215, 211
Men'shchikov, A.B., Tutukov, A.V., & Shustov, B.M. 1989, Sov. Astron., 33, 416
Merkle, F. 1986 in Second Workshop on ESO's Very Large Telescope, ESO Conf. Workshop Proc. No. 24, ed. S. D'Odorico & J.P. Swings (Garching: ESO), p. 443
Perrier, C., Chelli, A., & Zinnecker, H. 1987, in Interferometric Imaging in Astronomy, Proc NOAO-ESO Workshop, ed. J.W. Goad (Garching: ESO), p. 247
Rousset, G., Fontanella, J.C., Kern, P. Gigan, P., & Rigaut, F. 1990, A&A, 230, L29
Rigaut, F., Kern, P., Léna, P., Rousset, G., Fontanella, J.C., Gaffard, J.P., & Merkle, F. 1991, A&A, 250, 280
Rigaut, F., Gendron, E., Léna, P., Madec, P.Y., Couvée, X, & Rousset, G. 1992, in High Resolution Imaging by Interferometry, ESO Conf. and Workshop Proc. No. 39, ed. J.M. Beckers & F. Merkle (Garching: ESO), p. 1105
Rousset, G., et al. 1993, in Active and Adaptive Optics, ICO-16 Satellite Conf. ed. F. Merkle (Garching: ESO), p. 65
van Genderen, A.M., & Thé, P.S. 1984, Space Sci. Rev., 39, 317
Warren-Smith, R.F., Scarrot, S.M., Murdin, P., & Bingham R.G. 1979, MNRAS, 187, 761
Weigelt, G., & Ebersberger, J. 1986, A&A, 163, L5
Weigelt, G. et al. 1995, RevMexAASC, 2, 11
Whitelock, P.A., Feast, N.W., Carter, B.S., Roberts, G., & Glass, I.S. 1983, MNRAS, 203, 385